Carriers confinement study of GaNAsBi/GaAs QWs emitting at 1.3 and 1.55 μm

© A. Ben Nasr, M.M. Habchi, C. Bilel, A. Rebey¶, B. El Jani

University of Monastir, Faculty of Sciences,
Unité de Recherche sur les Hetero-Epitaxies et Applications,
5019 Monastir, Tunisia

(Получена 19 августа 2013 г. Принята к печати 3 июля 2014 г.)

Band structures of $GaN_{0.58y}As_{1-1.58y}Bi_y$/GaAs quantum wells (QWs) were studied using the band anticrossing model and the envelope function approximation. The confined states energies and the oscillator strengths of interband transitions were determined for well widths L_W and Bi composition y varying in the range of 4−10 nm and 0−0.07 respectively. The emissions 1.3 and 1.55 μm were reached for specific couples (L_W, y). The band anticrossing effect on the in-plane carriers effective mass has been investigated at $k = 0$. The absorbance spectra were calculated for QWs operating at 1.3 and 1.55 μm.

1. Introduction

$GaN_xAs_{1-x-y}Bi_y$ and related alloys have been developed during the last few years for optoelectronic device applications. They exhibit a large band gap reduction (less than 1 eV) which can be explained by the band anticrossing (BAC) model [1–4]. Moreover, by adjusting the bismuth and nitrogen amounts incorporated into GaAs, GaNAsBi can be lattice matched to GaAs like GaInNAs and GaNAsSb alloys [5,6]. Further, Janotti et al. [7] have demonstrated that Bi incorporation into GaNAs decreases further the N amount needed to achieve band gap lower than GaAs. This can compensate the nitrogen effects and improves the transport and optical properties of GaNAsBi alloys [8]. For these reasons, these alloys can be used especially in infrared diode lasers in optical fiber communications 1.3 and 1.55 μm [9]. However, the quantum wells (QWs) structures have attracted special attention due to their application in photodetectors and high efficiency solar cells. The most of studies were based on the electronic properties of GaNAs/GaAs and GaAsBi/GaAs QWs [10–15]. They have investigated the nitrogen effect on the confinement and the effective mass of electrons. Besides, the bismuth effect on optical properties of the GaAsBi/GaAs structures has also been studied. But only few of researches have concentrated on the study of the GaNAsBi/GaAs QWs. In fact, it has been demonstrated that $GaN_xAs_{1-x-y}Bi_y$/GaAs QWs is of type-I with a band offset ratio in the order of 70 : 30 [5]. In addition, they are considered more advantageous than GaInNAs/GaAs QWs emitting at 1.3 μm since they allow a good confinement of electrons and weak band gap temperature sensitivity [16]. However, so far, the optoelectronic properties of $GaN_xAs_{1-x-y}Bi_y$/GaAs QWs still provide a wide field of investigation especially the Bi and N effects on the confined levels, the in-plane carrier effective mass and the absorption coefficient.

¶ E-mail: ahmed.rebey@fsm.rnu.tn

The purpose of this work is to determine the quantified levels energy in $GaN_{0.58y}As_{1-1.58y}Bi_y$/GaAs QWs as well as the interband transitions for various Bi amounts (y) and wells widths (L_W). Our calculations have been concentrated on the fundamental transition T_{e1-h1}, between the ground heavy hole and electron subbands of the quantum well, leading to wavelength emission at 1.3 and 1.55 μm. The influence of Bi and N incorporation on the optoelectronic properties of the QWs has been investigated.

2. Theoretical framework

According to (16×16) BAC model, the bulk $GaN_xAs_{1-x-y}Bi_y$ band structure is described by the following Hamiltonian:

$$H_{16\times16} = \begin{pmatrix} & H^{mod}_{8\times8} & & V_{N(2\times8)} \\ & & & V_{Bi(6\times8)} \\ V_{N(8\times2)} & V_{Bi(8\times6)} & & H_{N,Bi(8\times8)} \end{pmatrix} \quad (1a)$$

where $H^{mod}_{8\times8}$ is the $(8 \times 8)\mathbf{k}\,\mathbf{p}$ matrix ($H^K_{8\times8}$), describing the band structure of bulk GaAs [18] and modified by adding the diagonal elements ΔE_{CBM}, ΔE_{VBM} and ΔE_{SO} (bands edges offset between GaAs and GaBi). relative to the Γ_6, Γ_8 and Γ_7 bands respectively. We also added two localized s-like states of N atoms and six localized p-like states of Bi atoms with basic functions identical to those describing the host GaAs. These states are represented by a diagonal (8×8) matrix (denoted $H_{N,Bi(8\times8)}$) formed by the positions of the N atoms level (E_N), the heavy/light hole levels of Bi atoms (E_{Bi}) and the corresponding spin orbit splitting level (E_{Bi-so}). $H_{N,Bi(8\times8)}$

can be written as:

$$H_{\mathrm{N,Bi}(8\times8)} = \begin{pmatrix} E_{\mathrm{N}} & 0 & 0 & 0 & 0 & 0 & 0 & 0 \\ 0 & E_{\mathrm{N}} & 0 & 0 & 0 & 0 & 0 & 0 \\ 0 & 0 & E_{\mathrm{Bi}} & 0 & 0 & 0 & 0 & 0 \\ 0 & 0 & 0 & E_{\mathrm{Bi}} & 0 & 0 & 0 & 0 \\ 0 & 0 & 0 & 0 & E_{\mathrm{Bi}} & 0 & 0 & 0 \\ 0 & 0 & 0 & 0 & 0 & E_{\mathrm{Bi}} & 0 & 0 \\ 0 & 0 & 0 & 0 & 0 & 0 & E_{\mathrm{Bi-so}} & 0 \\ 0 & 0 & 0 & 0 & 0 & 0 & 0 & E_{\mathrm{Bi-so}} \end{pmatrix} \quad (1b)$$

The Bi isoelectronic states E_{Bi} and $E_{\mathrm{Bi-so}}$ are located at 0.4 and 1.9 eV below the GaAs valence band edge [1], whereas the nitrogen state E_N is at about 0.23 eV above the GaAs conduction band edge [19]. Coupling between Bi isoelectronic localized states and extended valence band (VB)states was described by the matrix $V_{\mathrm{Bi}(6\times8)}$ which contains the coupling term $V_{\mathrm{Bi}}(y) = C_{\mathrm{Bi}}\sqrt{y}$. C_{Bi} is a fitting parameter equal to 1.55 eV [1]. We can write:

$$V_{\mathrm{Bi}(6\times8)} = \begin{pmatrix} 0 & 0 & V_{\mathrm{Bi}}(y) & 0 & 0 & 0 & 0 & 0 \\ 0 & 0 & 0 & V_{\mathrm{Bi}}(y) & 0 & 0 & 0 & 0 \\ 0 & 0 & 0 & 0 & V_{\mathrm{Bi}}(y) & 0 & 0 & 0 \\ 0 & 0 & 0 & 0 & 0 & V_{\mathrm{Bi}}(y) & 0 & 0 \\ 0 & 0 & 0 & 0 & 0 & 0 & V_{\mathrm{Bi}}(y) & 0 \\ 0 & 0 & 0 & 0 & 0 & 0 & 0 & V_{\mathrm{Bi}}(y) \end{pmatrix} \quad (1c)$$

For the coupling between the N localized states and the extended conduction band (CB) states, we associated the matrix $V_{\mathrm{N}(2\times8)}$ including a similar diagonal coupling term $V_{\mathrm{N}}(x) = C_{\mathrm{N}}\sqrt{x}$. C_{N} is a fitting parameter equal to 2.7 eV [19]. The matrix is expressed as follows:

$$V_{\mathrm{N}(2\times8)} = \begin{pmatrix} V_{\mathrm{N}}(x) & 0 & 0 & 0 & 0 & 0 & 0 & 0 \\ 0 & V_{\mathrm{N}}(x) & 0 & 0 & 0 & 0 & 0 & 0 \end{pmatrix} \quad (1d)$$

Note that there was no interaction between the Bi localized states and the CB states. The same thing has been noticed about interaction between the N localized states and the VB states.

In order to calculate the confined states in GaNAsBi/GaAs QWs basing on the envelope function approximation [20], the total Hamiltonian is given by:

$$H = H_{\parallel} + H_z, \quad \text{where } H_{\parallel} = -\frac{\hbar^2}{2m^*_{\parallel\, i}}\nabla^2_{\parallel}, \quad (2a)$$

$$\text{and } H_z = -\frac{\hbar^2}{2m^*_i}\nabla^2_z + U_i(z) \quad (2b)$$

are the Hamiltonian describing the carrier movement in the in-plane direction (x, y) and the Hamiltonian quantified along the z confinement direction respectively. $U_i(z)$ is the confining potential and $m^*_i(z)$ represents the carrier's effective mass in the well $(m^*_i(\mathrm{GaNAsBi}))$ and in the barrier $(m^*_i(\mathrm{GaAs}))$. In order to resolve Schrödinger equation (2b), we have applied the finite differential method to discrete the total Hamiltonian [21]. In this calculation, the envelope wave functions $\psi_n(z)$ satisfy to the boundary conditions at the interfaces $(z = 0)$ and $(z = L_W)$. These conditions are the continuities of the wave functions ψ_n and the courant of probability $\frac{1}{m_i}\left(\frac{d\psi_n}{dz}\right)$. Taking into account the boundary conditions verified by the confining potential and the effective mass:

$$U_i = \begin{cases} 0 & 0 \le z \le L_W \\ \Delta E_i = \begin{cases} \Delta E_c \text{ for } i = e \\ \Delta E_v \text{ for } i = hh \end{cases} & z < 0 \text{ or } z > L_W \end{cases}, \quad (3a)$$

$$m^*_i = \begin{cases} m^W_i = m^*_i(\mathrm{GaNAsBi}) & 0 \le z \le L_W \\ m^b_i = m^*_i(\mathrm{GaAs}) & z < 0 \text{ or } z > L_W \end{cases}. \quad (3b)$$

The confined energy levels $E_n(z)$ and their corresponding wave functions $\psi_n(z)$ are given respectively by the eigenvalues and the eigenvectors of H_z. Then, we solve the total Hamiltonian for various values of $k_{\parallel}$ in-plane wave vector. Note that our computing was done for $\mathrm{GaN}_x\mathrm{As}_{1-x-y}\mathrm{Bi}_y$ lattice matched to GaAs where N and Bi contents satisfy the condition: $x/y = 0.58$.

3. Results and discussion

The diagonalization of the (16×16) Hamiltonian requires the knowledge of the band gap energy, carrier effective mass and conduction and valence bands offsets of bulk $\mathrm{GaN}_x\mathrm{As}_{1-x-y}\mathrm{Bi}_y$. In fact, the BAC model has predicted a split-off of the conduction and valence bands due to the anticrossing interaction. The conduction band minimum (CBM) corresponds to the lower conduction subband energy E_{cb-}, while the valence band maximum (VBM) is described by the higher valence subband energy E_{hh+}. Then, the band gap energy E_g is given by the difference between E_{cb-} and E_{hh+}. The electron and holes effective masses were calculated using the density of states effective mass at the Brillouin zone center [19]. The conduction and valence band offsets are given by:

$$\Delta E_C = E_{C0}(\mathrm{GaAs}) - E_{cb-}(\mathrm{GaN}_{0.58y}\mathrm{As}_{1-1.58y}\mathrm{Bi}_y), \quad (4a)$$

$$\Delta E_V = E_{hh+}(\mathrm{GaN}_{0.58y}\mathrm{As}_{1-1.58y}\mathrm{Bi}_y) - E_{V0}(\mathrm{GaAs}), \quad (4b)$$

where $E_{C0}(\mathrm{GaAs}) = 1.423$ eV and $E_{V0}(\mathrm{GaAs}) = 0$ eV. Note that all calculations in this work were done at the temperature $T_0 = 300$ K. We have found that the band gap energy was reduced by roughly 198 meV/%Bi. Besides, for all compositions of N and Bi $(y \le 0.07,\ x \le 0.04)$, the conduction and valence band offset ratio was close to 70 : 30. In this way, a good agreement was obtained with results of Nacer et al. [5]. By integrating these parameters into the QWs calculations, we have determined the confined energy levels and the interbands transitions in $\mathrm{GaN}_{0.58y}\mathrm{As}_{1-1.58y}\mathrm{Bi}_y$/GaAs QWs for Bi compositions up to 0.07 and well widths L_W ranged from 4 to 10 nm. The

range of L_W was chosen according to the QWs confinement conditions expressed as follows:

$$L_{\min} = \pi\hbar/\sqrt{2m_e^w \Delta E_c}, \tag{5a}$$

$$L_{\max} = \frac{\lambda_{th}}{\pi}\cos^{-1}\sqrt{E_{\text{th}} \Big/ \left(\Delta E_c \frac{m_e^w}{m_e^b} + E_{th}\left(1 - \frac{m_e^w}{m_e^b}\right)\right)}, \tag{5b}$$

where $\lambda_{th} = 2\pi\hbar/\sqrt{2m_e^w k_B T}$ and $E_{th} = k_B T$ are the De Broglie thermal wavelength and the thermal energy, respectively. For this QW, we have found that $L_{\min} = 3.84$ nm and $L_{\max} = 11.53$ nm. Our calculations, performed at $k_{\parallel} = 0$, were illustrated in Fig. 1. At this point, the heavy and light holes levels were degenerated. As expected for the conduction and valence bands of bulk GaNAsBi, each confined level of GaNAsBi/GaAs QWs was divided into two sublevels (upper $E_{ei,hi}^{+}$ and lower $E_{ei,hi}^{-}$) because of the band anticrossing. But only the lower electron sublevels E_{ei}^{-} and the upper holes sublevels E_{ei}^{+} were confined in the QWs. Hence, the others sublevels E_{ei}^{-} and E_{ei}^{+} have been neglected and the sublevels and were denoted and respectively in the rest of work. Based on the selection rules, we have interested on the transitions $T_{\text{ie}-\text{jh}}$ where i and j are integers having the same parity. As can be seen, the number of interband transitions depends on y and L_W. It increases with both L_W and y. For $L_W \geq 7$ nm and $y > 0.03$, we can achieve four transitions denoted T_1, T_2, T_3 and T_4 corresponding to T_{e1-h1} (dash-dotted lines), T_{e1-h3} (solid lines), T_{e2-h2} (short-dashed lines) and T_{e2-h4} (dashed lines) respectively. As an example, the energy levels of $GaN_{0.033}As_{0.91}Bi_{0.058}$/GaAs QW with $L_W = 8$ nm is shown in the inset of Fig. 1. The energy diagram presents two electron subbands and four hole subbands giving rise to four transitions. The transition energy decreases when L_W and/or y(Bi) increases. This fact give rise to the emission 1.3 and 1.55 μm for different values of L_W coupled to specific values of y. As shown in Fig. 1, the couples (L_W, y) can be determined from the intercept (see symbols) of the fundamental transition (T_{e1-h1}) energies with the emission energies (horizontal dash-dotted lines corresponding to 0.80 eV (1.55 μm) and 0.95 eV (1.3 μm). Note that if L_W increases, the Bi or N contents decreases in order to keep the same transition energy. For example, a 10 nm QWs with $y = 0.037$ and $x = 0.021$ can emit at 1.3 μm. For the same nitrogen concentration, Kudrawiec et al. [22] have found that the $GaN_{0.02}As_{0.87}Sb_{0.11}$/GaAs QW with type-$I$ band gap alignment and a conduction band offset ratio of about 50% can reach the wavelength 1.3 μm. Furthermore, Harmand et al. [16] have proved experimentally that the 1.55 μm emission can be obtained with Sb and N compositions of 0.35 and 0.013, respectively. By comparing GaNAsSb/GaAs QWs with GaNAsBi/GaAs QWs, we found that they can achieve emission at longer wavelength (1.55 μm) with low nitrogen concentration unlike GaInAsN/GaAs QWs. Moreover, the incorporation of Sb into GaInAsN [23] and Bi into GaAsN improve their optical and structural properties. However, Bi impurities induce a huge band gap reduction as compared to Sb impurities due to the difference between the large mismatch ionization energies between Sb and Bi [1].

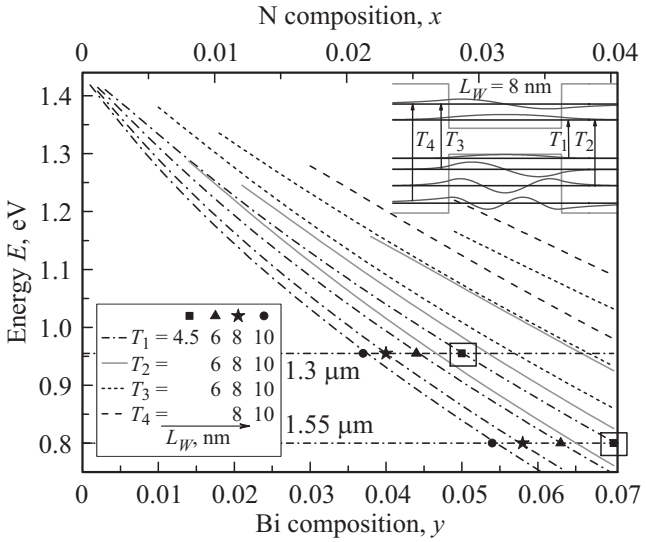

Figure 1. Interbands transitions energies in $GaN_{0.58y}As_{1-1.58y}Bi_y$/GaAs QWs as a function of Bi compositions up to 0.07 and well widths L_W ranging from 4 to 10 nm. Horizontal dash-dotted lines represent energies corresponding to wavelength emissions 1.3 and 1.55 μm. The interbands transitions are denoted T_1 (T_{e1-h1}, dash-dotted lines), T_2 (T_{e1-h3}, solid lines), T_3 (T_{e2-h2}, short-dashed lines) and T_4 (T_{e2-h4}, dashed lines). Symbols (squares, triangles, stars and circles) correspond to the couples (L_W, y) leading to the emission of T_1 at 1.3 and 1.55 μm. The inset shows the energy diagram with four transitions for GaAs/$GaN_{0.58y}As_{1-1.58y}Bi_y$/GaAs QW ($L_W = 8$ nm, $y = 0.058$) emitting at 1.55 μm.

For $L_W = 4.5$ nm, the $GaN_{0.03}As_{0.92}Bi_{0.05}$/GaAs and $GaN_{0.04}As_{0.89}Bi_{0.07}$/GaAs QWs give rise to emission at 1.3 and 1.55 μm respectively. Moreover, according to selection rules, only the transition T_{e1-h1} was permitted. Thus, $GaN_{0.03}As_{0.92}Bi0.05$/GaAs and $GaN_{0.04}As_{0.89}Bi_{0.07}$/GaAs QWs are more efficient than the others QWs. In general, the strength oscillator of the transition $_{ei-hj}$ writes [24]:

$$f_{ei-hj} = F_P/T_{ei-hj}|\Gamma_{ei-hj}|^2 \tag{6}$$

where $E_P = \frac{2}{m_0}|\langle u_c|p_z|u_v\rangle|^2$ is the Kane parameter calculated within the $k.p$ theory [20] and $|\Gamma_{ei-hj}| = |\langle\psi_{ei}|\psi_{hj}\rangle|$ is the modulus of the wave functions overlapping. We have found that the fundamental transition $f_{e1-h1} = 15.97$ emitting at 1.55 μm was larger than $f_{e1-h1} = 13.93$ emitting at 1.3 μm, L_W being equal to 4.5 nm. For the others QWs, f_{e1-h1} increases slowly when L_W increases, i. e y decreases. The oscillator strength achieves a value of 17.45 and 15.25 for $(L_W, y) = (10\,\text{nm}, 0.054)$ and $(10\,\text{nm}, 0.038)$ respectively. In fact, Eq. 6 shows that f_{e1-h1} varies proportionally to E_P and $|\Gamma_{e1-h1}|$. According to the BAC model prediction, the incorporation of few percent of bismuth and nitrogen into GaAs causes a decrease of E_g accompanied with an increase of Δ_{so} and m_e^* [25,10]. This means that E_P decreases with increasing Bi composition. The Kane parameter $E_P(y)$ values are equal to 14.227 and 14.617 eV for $y = 0.07$ and 0.05 respectively. Furthermore, $|\Gamma_{e1-h1}|$

decreases with the increase of y and it increases slowly with increasing of L_W. As an example, $|\Gamma_{e1-h1}|$ calculated for the couples $(L_{W,y}) = (4.5\,\text{nm}, 0.07)$ and $(8\,\text{nm}, 0.07)$ were close to 0.95 and 0.97 respectively. Therefore, we assume that the variation of f_{e1-h1} with L_W can be neglected.

Fig. 2, *a* shows the energy levels of $GaN_{0.04}As_{0.89}Bi_{0.07}$/GaAs QW emitting at 1.55 μm for $L_W = 4.5$ nm. The corresponding wave functions were also plotted. The origin of energies was taken at GaAs valence band edge. The discontinuity of bands ΔE_C and ΔE_V in $GaN_{0.04}As_{0.89}Bi_{0.07}$/GaAs QWs were 0.536 and 0.297 eV respectively. E_g was reduced from 1.423 eV in GaAs barrier to 0.601 eV in $GaN_{0.04}As_{0.89}Bi_{0.07}$ well. Since N and Bi impurities have produced a huge shift of the conduction and valence band edge, both electrons and holes were confined in the quaternary alloy. As a result, the band alignment of our QWs was of type-*I*. As shown in Fig. 2, *a*, we have obtained one electron confined state $e1$ located at 1.055 eV and two heavy hole confined states $h1$ and $h2$

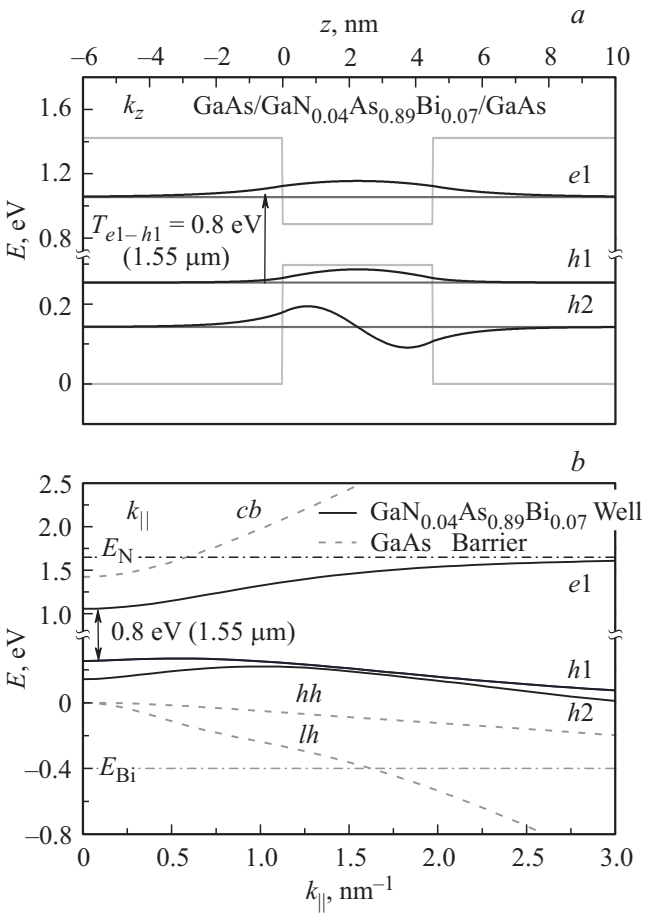

Figure 2. *a* — energy levels in $GaN_{0.04}As_{0.89}Bi_{0.07}$/GaAs QWs emitting at 1.55 μm for $L_W = 4.5$ nm. The corresponding wave functions were plotted. *b* — confined electron and holes levels in $\mathbf{k}_{||}$ direction for $GaN_{0.04}As_{0.89}Bi_{0.07}$/GaAs QWs (solid lines). The dashed lines present the band structure of bulk GaAs barrier, calculated in $\mathbf{k}_{||}$ direction. The dash-dotted lines show the N and Bi localized levels in GaAs (E_N and E_{Bi}). The indices cb, hh and lh denote respectively conduction band electrons, heavy holes and light holes bands.

situated at 0.254 eV and 0.143 eV respectively. In the case of $GaAs_{0.93}Bi_{0.07}$/GaAs QWs, ΔE_C is very small; it takes a value of 0.147 eV. In fact, Bi impurities incorporation into GaAs has no effect on the conduction band edge and CBM shift observed comes only from the discontinuity of bands between GaAs and GaBi. Then, electrons were not confined in the conduction band. In the other hand, ΔE_V is at about 0.297 eV and this structure presents two holes confined states $h1$ and $h2$ located at the same values obtained in the case of $GaN_{0.04}As_{0.89}Bi_{0.07}$/GaAs QWs. This means that nitrogen incorporation doesn't affect valence band. The fundamental transition calculated for this structure was at about 1.02 eV. Due to the interaction between the nitrogen state and the conduction band of GaAs for $GaN_{0.04}As_{0.96}$/GaAs QWs, CBM of $GaN_{0.04}As_{0.96}$ shifts down from 1.423 eV (GaAs) to 0.813 eV. We have found that only one electron confined state exists in this structure and it was located at 1.127 eV. ΔE_C was equal to 0.16 eV and $\Delta E_V = 0$ eV. Thus, no holes confined state was found in $GaN_{0.04}As_{0.96}$/GaAs QWs.

Fig. 2, *b* represents the band structure of the electron and holes confined levels in $\mathbf{k}_{||}$ direction for $GaN_{0.04}As_{0.89}Bi_{0.07}$/GaAs QWs emitting at 1.55 μm with 4.5 nm well width. The dashed lines present the band structure of bulk GaAs barrier (cb, hh and lh), calculated in $k_{||}$ direction. The dash-dotted lines show the nitrogen (E_N) and bismuth (E_{Bi}) localized levels. The interaction between E_N and the conduction band edge causes a strong non-parabolicity in the dispersion relation. The electron levels were located below E_N. They retain the localized character of E_N for high values of $\mathbf{k}_{||}$. When N content increases, the electron level shifts down. The same behavior was observed in the band structure of 1.3 μm InGaAsN/GaAs QWs laser [26]. Turning to the confined heavy-holes levels, we have found that they were shifted upward with increasing Bi content. Besides, they have an electronlike dispersion at small values of $\mathbf{k}_{||}$. This subband warping has been observed in the valence subband dispersion of 100 Å $In_{0.16}Ga_{0.84}As_{0.14}Sb_{0.86}/Al_{0.4}Ga_{0.6}Sb$ and $GaAs/Al_{0.2}Ga_{0.8}As$ QWs [18,27]. It originates from the interaction between the different subbands. Note that the warping of the holes subbands can modify the in-plane carrier effective mass values.

We present in Fig. 3 the electron and holes in-plane effective masses $m^*_{||\,i}$ ($i = e1$, $h1$ and $h2$) calculated as a function of Bi composition coupled to well width in $GaN_{0.58y}As_{1-1.58y}Bi_y$/GaAs QWs emitting at 1.3 and 1.55 μm. All effective masses are in free electron mass unit m_0. The inset shows a schematic structure of the subbands energies for the QWs in k_z and $k_{||}$ directions. $m^*_{||\,i}$ were calculated as the second derivative of the corresponding confined level in the vicinity of the edge ($k_{||} = 0$). Note that $m^*_{||e1}$ was slowly increased with the increasing of y and the decreasing of L_W. Besides, for the whole range of y, the value of $m^*_{||e1}$ remains at around $0.1m_0$. This fact was in good agreement with the result of PR measurements published by Wu et al. [11]. They have found that, for $0.012 \leqslant x \leqslant 0.028$ and $L_W < 10$ nm,

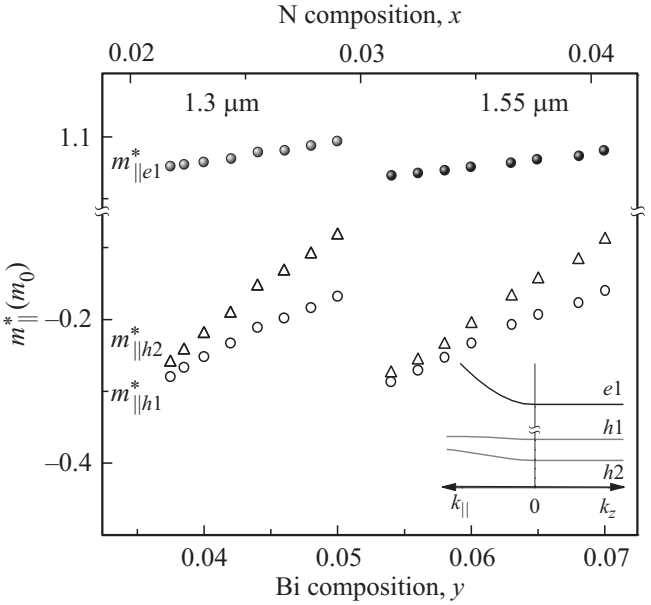

Figure 3. In-plane carrier effective mass $m^*_{\|i}$ ($i = e1$ (full sphere), $h1$ (open circles) and $h2$ (open triangles)) calculated, in $GaN_{0.58y}As_{1-1.58y}Bi_y$/GaAs QWs emitting at 1.3 and 1.55 μm as a function of y coupled to L_W. The inset shows schematic subband energies of $GaN_{0.58y}As_{1-1.58y}Bi_y$/GaAs QWs in $\mathbf{k}_z$ and $\mathbf{k}_\|$ directions.

the effective mass in GaN_xAs_{1-x}/GaAs QWs took a value of about $0.11\,m_0$. Using a 10-band $\mathbf{k}\cdot\mathbf{p}$ model, Stanko et al. [28] have confirmed the in-plane effective mass behavior in GaN_xAs_{1-x}/GaAs QWs with well width between 2 and 25 nm and N composition of 1–4%. We also confirm the results published for InGaAsN QWs [29]. In fact, $m^*_{\|e1}$ starts to increase rapidly for a fixed L_W when y increases in order to achieve its maximum. After that, it decreases slowly with increasing y. The effective mass of heavy and light holes can eventually become negative if hh_n (or lh_n) subband has a positive curvature near $k_\| = 0$ [20]. In other words, this behavior can be explained by the electronlike dispersion of the confined holes levels in the vicinity of the edge. We have also remarked that $m^*_{\|h2}$ was higher than $m^*_{\|h1}$ but both increase with the increase of y (i. e the decrease of L_W). The values of $m^*_{\|e1}$, $m^*_{\|h1}$ and $m^*_{\|h2}$ calculated for the QWs emitting at 1.3 μm were close to those of the QWs emitting at 1.55 μm which means that they present almost the same band dispersion in $\mathbf{k}_\|$-direction.

Fig. 4, *a* and 4, *b* show the absorbance spectra $A(E)$ of three $GaN_{0.58y}As_{1-1.58y}Bi_y$/GaAs QWs operating at 1.55 and 1.3 μm with different values of well width and Bi composition. Note that vertical arrows indicate band gap energy $E_{\text{bulk}g}$ of the $GaN_{0.58y}As_{1-1.58y}Bi_y$ bulk quaternary alloys lattice matched to GaAs. $E_g^{\text{bulk}}(y)$ are equal to 0.692, 0.601 and 0.764 eV for $y = 5.8$, 7 and 5% respectively. We chose to present absorbance spectra instead of those of absorption coefficient α_{abs} to remove the width well effect in the discussion about the order of magnitude of the absorbance. For a rectangular finite type-I quantum well of width L_W with non-exacitonic absorption, the interband optical absorbance may be written as follows [20,30,31]:

$$A = \alpha_{abs} L_W = \pi\alpha/n_r E \sum_{i,j} \mu^*_{ei-hj} T_{ei-hj} \Theta(E - T_{ei-hj}) \quad (7)$$

where $\Theta(E)$ is called the Heaviside step function and $1/\mu^*_{ei-hj} = 1m^*_{\|ei} + 1m^*_{\|hj}$ is the reciprocal reduced mass for the valence and conduction subbands. μ^*_{ei-hj} were determined for the studied QWs structures based on the carrier effective mass calculations performed in the previous section. We found that μ^*_{e1-h1} values are equal to 0.1028, 0.2022 and $0.2314m_0$ for Bi composition $y = 5.8$, 7 and 5% respectively. Note that the sommation $\sum_{i,j}$ is performed upon all the allowed interband transitions to satisfy the selection rules of the quantum numbers of the initial and the final subbands. The fine structure constant α is equal to $e^2/4\pi\varepsilon_0\hbar c = 1/137$ where e is the electron charge, c is the speed of light, is the Planck's constant, ε_0 is the vacuum permittivity and n_r is the real part of surrounding refractive index. Up to now, the refractive index of GaNAsBi alloys is an unknown parameter. However, since small nitrogen and bismuth amounts were incorporated into GaAs and $GaN_{0.58y}As_{1-1.58y}Bi_y$ well was lattice matched to GaAs (no strain effect), we have assumed as first approximation that they have the same refractive indices. However, the real refractive index n_r of GaAs varies slightly

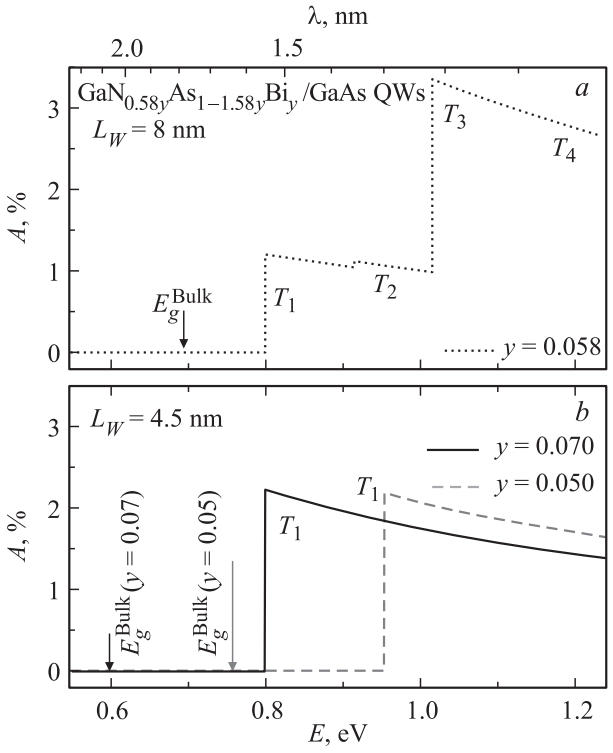

Figure 4. The variation of the absorbance $A(\%)$ of $GaN_{0.58y}As_{1-1.58y}Bi_y$/GaAs QWs as a function of energy E (or wavelength) for (*a*) well width $L_W = 8$ nm and Bi composition $y = 5.8\%$ (*b*) $L_W = 4.5$ nm and $y = 7\%$ and 5%. Note that vertical arrows indicate band gap energy of the $GaN_{0.58y}As_{1-1.58y}Bi_y$ bulk quaternary alloys lattice matched to GaAs.

with energy. $n_r(E)$ rises monotonously from 3.31 to 3.51 in the range 0.55−1.24 eV (1−2.25 μm). Analysis of Fig. 4 shows that the absorbance A is described by Heaviside functions centered on the interband transitions unlike the case of the direct band-to-band transition in bulk semiconductor (three-dimensional materials) where the dependence of the absorbance on the incident photon energy is given by [32]: $A_{\text{bulk}} \propto \sqrt{E - E_g^{\text{bulk}}}/(n_r E)$. Besides, for QWs operating at 1.55 μm, the absorbance of well with width $L_W = 4.5$ nm reaches its maximum of 2.21% at the fundamental transition. This value is almost twice the calculated magnitude ($A = 1.20\%$) when $L_W = 8$ nm. This behavior can be explained by the rise of optical transitions number from one to four interband transitions. The curve $A(E)$ of structure with well width equal to 8 nm has an absolute maximum of 3.34% at the third transition $T_{e2-h2} = 1.016$ eV ($\sim 1.22\,\mu$m). We also note that the energy difference ($\Delta E = T_{e1-h1} - E_g^{\text{bulk}}$) between the fundamental transition in QW and the bandgap in bulk has almost doubled from 0.11 to 0.20 eV by decreasing the well widths from 8 to 4.5 nm. On the other hand, Fig. 4, *b* shows the absorbance spectra of $GaN_{0.04}As_{0.89}Bi_{0.07}$/GaAs and $GaN_{0.03}As_{0.92}Bi_{0.05}$/GaAs quantum wells (with $L_W = 4.5$ nm) having single transitions at 1.55 and 1.3 μm respectively. The emission wavelengths do not affect significantly the maximum value of absorbance nor the difference of energy ΔE. Then, the magnitudes of A and ΔE retain values around 2.2% and 0.2 eV respectively.

4. Conclusions

In summaries, we have presented a theoretical study of the optoelectronic properties of GaNAsBi/GaAs QWs. Our calculations show that, due to the band anticrossing, the interband transitions energy shift down with increasing Bi and N compositions. This result improves that $GaN_{0.58y}As_{1-1.58y}Bi_y$/GaAs QWs can reach the wavelength 1.3 and 1.55 μm by adjusting the Bi or N contents and the well width. The dispersion of the confined electron and holes levels has been determined along the in-plane direction. The carrier effective masses of the confined states were determined for different values of Bi composition coupled to the well width. We have calculated the oscillator strength and the absorbance spectra of the fundamental transition for $GaN_{0.03}As_{0.92}Bi_{0.05}$/GaAs and $GaN_{0.04}As_{0.89}Bi_{0.07}$/GaAs QWs emitting at the telecommunication wavelengths.

We gratefully acknowledge financial support from the DGRST-Tunisia.

References

[1] K. Alberi, J. Wu, W. Walukiewicz, K.M. Yu, O.D. Dubon, S.P. Watkins, C.X. Wang, X. Liu, Y.-J. Cho, J. Furdyna. Phys. Rev. B, **75**, 045 203 (2007).
[2] W. Shan, K.M. Yu, W. Walukiewicz, J. Wu, J.W. Ager III, E.E. Haller. J. Phys. Condens. Matter, **16**, S3355 (2004).
[3] Y.N. Qiu, J.M. Rorison. Appl. Phys. Lett., **87**, 081 111 (2005).
[4] J-Y. Duboz. Phys. Rev. B, **75**, 045 327 (2007).
[5] S. Nacer, A. Aissat, K. Ferdjani. Optical Quant. Electron., **40**, 677 (2008).
[6] P. Wei, S. Tixier, M. Chicoine, S. Francoeur, A. Mascarenhas, T. Tiedje, F. Schiettekatte. Nucl. Instrum. Meth. Phys. Res. B, **219**, 671 (2004).
[7] A. Janotti, S.-H. Wei, S.B. Zhang. Phys. Rev. B, **65**, 115 203 (2002).
[8] E.C. Young. (Ph.D. Thesis, University of British Columbia, 2006).
[9] W. Huang, K. Oe, G. Feng, M. Yoshimoto. J. Appl. Phys., **98**, 053 505 (2005).
[10] C. Skierbiszewski, S.P. Lepkowski. P. Perlin, T. Suski, W. Jantsch, J. Geisz. Physica E, **13**, 1078 (2002).
[11] J. Wu, W. Shan, W. Walukiewicz, K.M. Yu, J.W. Ager III, E.E. Haller, H.P. Xin, C.W. Tu. Phys. Rev. B, **64**, 085 320 (2001).
[12] H. Dumant, L. Auvray, Y. Monteil, F. Saidi, F. Hassen, H. Maaref. Optical Mater. **24**, 303 (2003).
[13] S. Imhof, C. Buckers, A. Thranhardt, J. Hader, J.V. Moloney, S.W. Koch. Semicond. Sci. Technol., **23**, 125 009 (2008).
[14] Y.I. Mazur, V.G. Dorogan, M. Schmidbauer, G.G. Tarasov, S.R. Johnson, X. Lu, S-Q. Yu, Z.M. Wang, T. Tiedje, G.J. Salamo. Nanotechnology, **22**, 375 703 (2011).
[15] J. Hwang, J.D. Phillips. Phys. Rev. B, **83**, 195 327 (2011).
[16] J.C. Harmand, G. Ungaro, J. Ramos, E.V.K. Rao, G. Saint-Girons, R. Teissier, G. Le Roux, L. Largeau, G. Patriarche. J. Cryst. Growth, **227**, 553 (2001).
[17] M.M. Habchi, A. Ben Nasr, A. Rebey, B. El Jani, Infrared Physics & Technology **61**, 88 (2013).
[18] A.T. Meney, B. Gonul, E.P. O'Reilly. Phys. Rev. B, **50**, 10 893 (1994).
[19] J. Wu, W. Shan, W. Walukiewicz. Semicond. Sci. Technol., **17**, 860 (2002).
[20] G. Bastard. *Wave mechanics applied to semiconductor heterostructures* (Les Editions de Physique, Les Ulis Cedex, France, 1990).
[21] D. Ahn, S.L. Chuang, Y.-C. Chang. J. Appl. Phys., **64**, 4056 (1988).
[22] R. Kudrawiec, K. Ryczko, J. Misiewicz, H.B. Yuen, S.R. Bank, M.A. Wistey, H.P. Bae, J.S. Harris. Appl. Phys. Lett., **86**, 141 908 (2005).
[23] H.B. Yuen, S.R. Bank, H. Bae, A.M. Wistey, J.S. Harris. J. App. Phys., **99**, 093 504 (2006).
[24] S.C.P. Rodrigues, G.M. Sipahi, E.F. da Silva, jr. Microelectron. J., **36**, 434 (2005).
[25] B. Fluegel, S. Francoeur, A. Mascarenhas. Phys. Rev. Lett., **97**, 067 205 (2006).
[26] S. Tomić, E.P. O'Reilly, R. Fehse, S.J. Sweeney, A.R. Adams, A.D. Andreev, S.A. Choulis, T.J.C. Hosea, H. Riechert. J. Selected Topics Quant. Electron., **9**, 1228 (2003).
[27] A. Lucio Claudio, P. Alfredo, B. Franco. Phys. Rev. B,**36**, 5887 (1987).
[28] S. Tomić, E.P. O'Reilly, P.J. Klar, H. Grüning, W. Heimbrodt, W.M. Chen, I.A. Buyanova. Phys. Rev. B,**69**, 245 305 (2004).
[29] S. Tomić, E.P. O'Reilly. Phys. Rev. B, **71**, 233 301 (2005).
[30] H. Fang, H.A. Bechtel, E. Plis, M.C. Martin, S. Krishna, E. Yablonovitch, A. Javey, P. Natl. Acad. Sci. USA. **110**, 11688 (2013).
[31] S. Kasap, P. Capper (Eds.), Springer Handbook of Electronic and Photonic Materials (Springer, 2006), 1026-1029, e-ISBN: 0-387-29185-7.
[32] P.K. Basu, Theory of Optical Process in Semiconductors Bulk and Microstructures, (Clarendon Press, Oxford, 1997).

Редактор Т.А. Полянская